

## Oxygen Saturation as a Strategy to Mitigate User-Induced Variation in Tomographic Volumetric Additive Manufacturing

Carl Sander Kruse\*<sup>a,c</sup>, Nicole Pellizzon<sup>a</sup>, Roozbeh Salajeghe<sup>a</sup>, Jon Spangenberg<sup>a</sup>, Frieder  
Lucklum<sup>b,c</sup>, Aminul Islam<sup>a,c</sup>

<sup>(a)</sup> Department of Civil and Mechanical Engineering, Technical University of Denmark

<sup>(b)</sup> Department of Electrical and Photonics Engineering, Technical University of Denmark

<sup>(c)</sup> Centre for Acoustic-Mechanical Microsystems (CAMM), Technical University of Denmark

<sup>(\*)</sup> Corresponding author: [cgskr@dtu.dk](mailto:cgskr@dtu.dk)

### Abstract

Tomographic Volumetric Additive Manufacturing (TVAM), also known as Computed Axial Lithography (CAL), offers unparalleled geometric freedom and speed but faces challenges with inconsistency caused by user-induced variation. This paper presents novel insights into mitigating user-induced variation by addressing manual preparation of the photopolymer and print vials. Two different methods of preparing the print vials are employed to investigate the oxygen concentration within a batch of photopolymer, each followed by ten consecutive prints of the same geometry and subsequent analysis of the polymerization progressions captured through in-situ monitoring. Results show that the oxygen concentration of the photopolymer is highly dependent on the method of preparation, and that promoting oxygen diffusion directly in the print vial to saturate the photopolymer before printing significantly increases the consistency of the printing process. Using this methodology, print vials exhibited a curing onset variation of only a few seconds, significantly enhancing the uniformity of the printed parts.

### Introduction

Tomographic Volumetric Additive Manufacturing (TVAM), also known as Computed Axial Lithography (CAL), is a new Additive Manufacturing (AM) technique initially presented in 2017 and subsequently popularized in 2019 by Kelly et al. [1,2]. In TVAM, rather than printing geometries layer-by-layer, geometries are instead printed on a volumetric basis meaning they materialize in their entire volume simultaneously, which leads to support-free printing and smooth surfaces [2, 3, 4, 5], easy overprinting [2, 6], as well as isotropic material properties for a wide range of materials including acrylates [2, 3], ceramics [5, 7], thiol-enes [8, 9], and cell-laced hydrogels [10, 11]. Additionally, the manufacturing time is reduced to only a few minutes, or even a few seconds [3, 12, 13], as TVAM is effectively the equivalent of printing all layers at once compared to traditional layer-by-layer AM techniques. However, despite TVAM showing great potential and while significant advancements have already been made within the field across the many engineering disciplines it spans, the technique is facing challenges with inconsistency due to user-induced variation, which is limiting its widespread adoption.

The volumetric printing capability is achieved by projecting a sequence of tomographic light patterns into a rotating cylindrical print vial filled with a high-viscosity photopolymer exhibiting non-linear curing, as seen in Fig. 1. After only a few revolutions of the print vial, the superposition of the projected light patterns results in a 3D energy dose that makes the photopolymer cure in the desired shape when the curing threshold is reached. Once cured, the printed part can be extracted from the cylindrical print vial and cleaned of any residual uncured photopolymer prior to post-curing, yielding the result seen in Fig. 2C. The non-linear curing

behaviour of the photopolymer is caused by the presence of inhibiting species dissolved within the photopolymer, combined with the photoinitiator used having a low absorption at the specified projection wavelength. The dissolved inhibitor sets a critical dose threshold by providing an inhibition period where free radicals are scavenged at a much faster rate than they are formed and react with the monomers, which allows for the 3D energy dose to build up without inadvertently curing the photopolymer in unwanted regions within the print vial. Once the inhibitor has been sufficiently depleted by the 3D energy dose, the polymerization and subsequent crosslinking reactions take place, after which the projection must be stopped once the part has fully formed.

Due to the nature of the printing process, determining the time at which to stop the projection is therefore critical to the geometric fidelity of the printed parts, as too short a projection time will result in the geometry not fully forming, while too long a projection time will cause overcuring, as regions outside the 3D energy dose will also begin to exceed the critical dose threshold. In layer-by-layer AM techniques, the print time mostly depends on the size, volume and vertical resolution of the printed part. However, in TVAM, the print time predominantly depends on the morphology of the part itself due to the nature of the printing process, which makes determining the optimal print time inherently difficult.

Traditionally within the field, the time at which to stop the projection has been determined manually by continuing the projection for a short period of time after the first signs of curing had been observed, and then stopping once the part appears to have fully formed. However, as this approach is heavily influenced by the subjectivity of the user since the polymerization progression is difficult to see by eye, it was soon realized that better and more objective methods were needed. In response, Loterie et al. [3] presented an approach based upon in-situ monitoring, where a shadowgraphy imaging system was used to provide information about the polymerization progression of a print, which was then used for spatial adjustment of the tomographic light patterns, allowing for a second, more accurate print to be made using the same print time. This idea was later expanded on by Li et al. [14] using a Schlieren imaging system to also track the degree of curing, yielding even more information about the polymerization progression. A different approach was introduced by Orth et al. [15,16], where isotropic light scattering caused by the photopolymer curing was used for on-the-fly metrology and as a metric to determine when a print should be stopped or how it should be improved, while also making it easier to observe the printing process by eye. Further advancing the field, Weisgraber et al. [17] developed the digital twin, VirtualVAM, capable of simulating the polymerization progression during prints, which has been proven to qualitatively match experimental results. However, timestamps from the digital twin and the experimental results have shown to differ, indicating that in its current state, VirtualVAM alone cannot be used to determine the optimal print time. Similarly, the Energy Threshold model presented by Salajeghe et al. [18] tracks energy accumulation over time within the photopolymer. However, as their study only considers one revolution of the print vial, this likewise only provides a qualitative indication of how the polymerization will progress, but not a definitive time at which to stop the projection to get the most optimal print quality.

Regardless of whether the time at which to stop the projection is determined manually, through in-situ monitoring, or by means of simulation, once the optimal print time has been established for a particular geometry, any consecutive print of the same geometry using this print time should ideally result in the same consistent polymerization progression and print quality. However, previous experience has shown that this is not always the case, which is believed to be a consequence of user-induced variation. This inconsistency has proven to be

especially problematic when it comes to demonstrating presumed improvements to the printing process emerging from research within the field, as comparison of identical geometries printed with, for example, changes to the tomographic light patterns, cannot be performed objectively on an equal basis. Put simply, without a proven, repeatable, and consistent printing process, it becomes difficult to conclude if a resulting change in print quality, whether positive or negative, can be attributed directly to the presumed improvement, or if it simply falls within the variability of the printing process. Establishing well-defined procedures that ensure consistency in the printing process is therefore highly important and will allow researchers to draw more accurate conclusions faster, thereby accelerating research within the field.

The printing procedure can overall be divided into three steps: 1) Preparation, where the photopolymer is prepared and the print vials are filled, 2) Printing, where the print vials are exposed to the sequence of tomographic light patterns while rotating, and 3) Post-processing, where the printed geometries are carefully extracted from the print vials and then cleaned using a solvent prior to post-curing. When it comes to the first of these three steps, it is believed that the manual work involved in mixing the photopolymer and preparing the print vials makes it a significant source of user-induced variation. To consistently achieve the same print quality for geometries while using the same print time, it naturally follows that the photopolymer must exhibit consistent material properties, such that the inhibition period and optimal print time is uniform for all print vials once filled. For photopolymers such as the Bisphenol A glycerolate diacrylate and Poly(ethylene glycol) diacrylate (BPAGDA/PEGDA) mixtures presented by Kelly et al. [2], the inhibitory effect is achieved by deliberately letting oxygen diffuse into the photopolymer after mixing. In their publication, this procedure is described as storing the photopolymer in an open container exposed to room air for several days with the aim of ensuring sufficient and uniform oxygen concentration throughout the photopolymer before the print vials are filled. However, there are no dedicated studies in literature investigating whether, or how, this is achieved for the entire batch of photopolymer. Should the oxygen concentration prove not be uniform, this could help explain the inconsistency that is currently observed as it would cause the inhibition period and optimal print time to vary between print vials as they are filled, effectively making the printing process unpredictable and a matter of trial and error.

In this paper, two different methods of preparing the print vials have been employed with the objective of investigating the oxygen concentration within a batch of photopolymer as well as quantifying its effect on the consistency of the printing process. The first method seeks to characterize the uniformity of the oxygen concentration throughout the container in which the batch of photopolymer is stored, while the second method seeks to promote oxygen diffusion directly in the print vials with the aim of ensuring that the photopolymer becomes fully saturated before printing. After preparation of the print vials, ten consecutive prints of the same geometry were performed for each of the two methods, followed by an analysis of their respective polymerization progressions captured through in-situ monitoring. In Section 2, a detailed description of the methods used in mixing the photopolymer and preparing the print vials is provided, along with an overview of the experimental setup used for printing. In Section 3, the results obtained from the different methods of preparing the print vials are presented and discussed, and finally, a conclusion is drawn based on the findings.

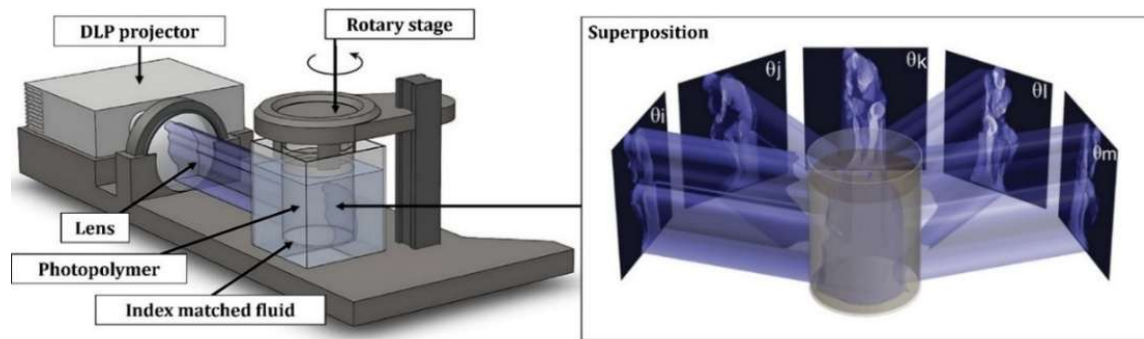


**Figure 1:** TVAM setup and working principle. A DLP projector sequentially projects a set of tomographic light patterns into a rotating vat filled with photopolymer. As the images are superimposed over time, the accumulated light dose cures the photopolymer into the desired 3D object. Figure adapted from [2] with permission.



**Figure 2:** *The Thinker* used as reference geometry in this work. (A) Sculpture at *Glyptoteket* in Copenhagen, (B) STL-file used for generating the projection image set, (C) Post-cured print. *The Thinker* was chosen as the reference geometry, as it is a common benchmark geometry within the field of TVAM due to its recognizable form and geometric complexity.

## **Methodology and experimental setup**

In preparation for the study, a batch of 75:25 wt% BPAGDA/PEGDA with 10.4 mM CQ/EDAB photoinitiator added was mixed and subsequently stored in a 1000 ml laboratory glass bottle covered with aluminum foil. After filling the glass bottle, it was intentionally left open for a week to allow atmospheric oxygen to diffuse into the photopolymer, in accordance with the method established by Kelly et al. [2]. However, since the surface area available for diffusion had been small relative to the total volume of photopolymer, it was questioned whether the oxygen concentration had in fact become uniform, or if a slight oxygen concentration gradient going from the top to the bottom of the glass bottle could potentially have formed during this time.

To address these questions, two experiments each employing different methods of preparing the print vials were performed to investigate the oxygen concentration within the batch of photopolymer as well as quantifying its effect on the consistency of the printing process. Normally, the print vials have been filled manually by pouring the photopolymer directly from the glass bottle, however, as this method would disturb the potential oxygen concentration gradient, instead, an automated machine capable of filling the print vials while keeping the glass bottle vertically was developed, as seen in Fig. 3A. The machine features a simple X/Z gantry system that can fill six Ø30 mm borosilicate glass test tubes at a time using a peristaltic pump connected to a long filling nozzle in one end, and a metal straw going to the bottom of the glass bottle in the other end. The filling nozzle is equipped with a pneumatic tube, which allows for flushing the print vials with pure nitrogen gas during filling. This displaces any atmospheric oxygen that may be present, thereby helping to preserve the effect of the oxygen concentration gradient on the consistency of the printing process, should it exist. In the first experiment, the print vials were filled using the automated filling machine while being flushed with pure nitrogen gas to prevent any oxygen transfer during the process. Once filled, the print vials were immediately sealed, heated in hot water to remove air bubbles, and then allowed to cool down to room temperature before being used for printing in random order.

In the second experiment, the print vials were also filled using the automated filling machine, however, without being flushed with pure nitrogen gas or immediately sealed. Instead, once filled, the print vials were oriented horizontally and rotated to coat the internal walls and induce a large surface area, as seen in Fig. 3B, thereby promoting oxygen diffusion directly in the print vials with the aim of ensuring that the photopolymer becomes fully saturated before printing. After this procedure, the print vials were sealed, heated in hot water to remove air bubbles, and then allowed to cool down to room temperature before being used for printing in random order.

The experiments were performed on a purpose-built TVAM printing setup as seen in Fig. 3C-D, consisting of a PRO4500 UV (405 nm) DLP-projector from Wintech Digital used together with an AL50100-G aspheric lens from Thorlabs for collimation of the projected light, resulting in a projected pixel size of  $44 \times 44 \mu\text{m}$  and a 10 mm depth of field. The print vials were rotated using a belt-driven RB-90-1-D rotary stage from Newmark Systems while being submerged in 75:25 wt% BPAGDA/PEGDA without photoinitiator added acting as the refractive index matched fluid. For in-situ monitoring and recording during each print, a shadowgraph imaging system was implemented consisting of two GoldTL™ 55-348 telecentric lenses from Edmund Optics used in combination with a Basler Ace acA2440-75uc camera and a red (625 nm) SL162 LED from Advanced Illumination. For both experiments, *The Thinker* was used as the reference part to be printed, as seen previously in Fig. 2. The corresponding sequence of tomographic light patterns was generated using the Object-Space Model

Optimization algorithm (OSMO) [19] in VAMToolbox [20], at a vertical resolution of 570 pixels corresponding to a projected height of 25 mm. The OSMO algorithm was chosen as it provides a large process window as seen in Fig. 4, i.e., a large contrast between the in-part and out-of-part dose. The large process window helps to improve the robustness of the printing process as it allows for slight errors in dose delivery and material response while still achieving ideal curing, meaning that if the process window is hit, any printed geometry will in theory achieve its most optimal print quality for the given TVAM printing setup. After printing, the parts were carefully extracted from the print vials and then post-processed accordingly.

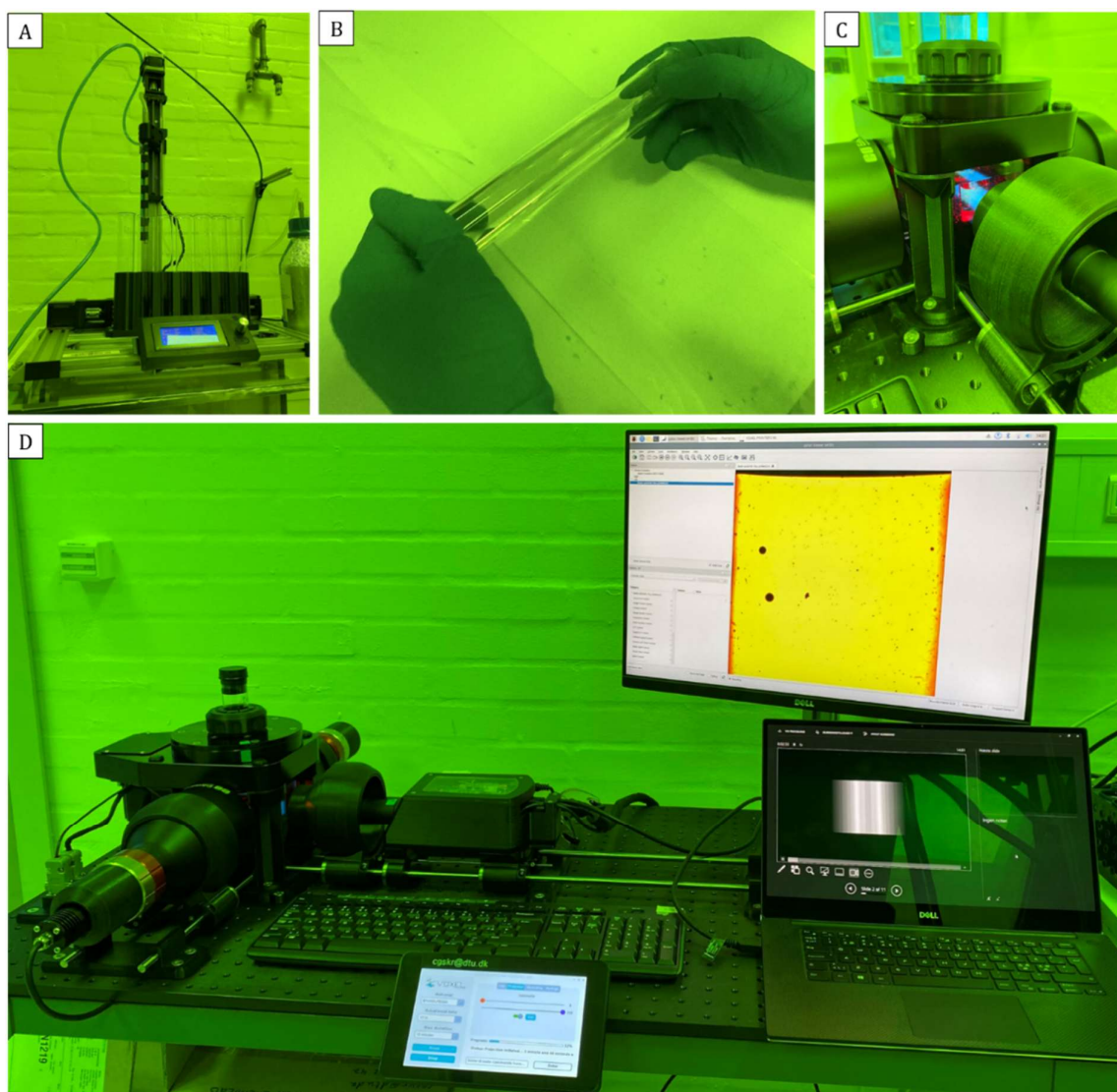


**Figure 3:** Experimental setup. (A) Automated filling machine with pneumatic tube, (B) Print vial oriented horizontally and rotated to promote oxygen diffusion, (C) Closeup while printing, (D) TVAM printer.

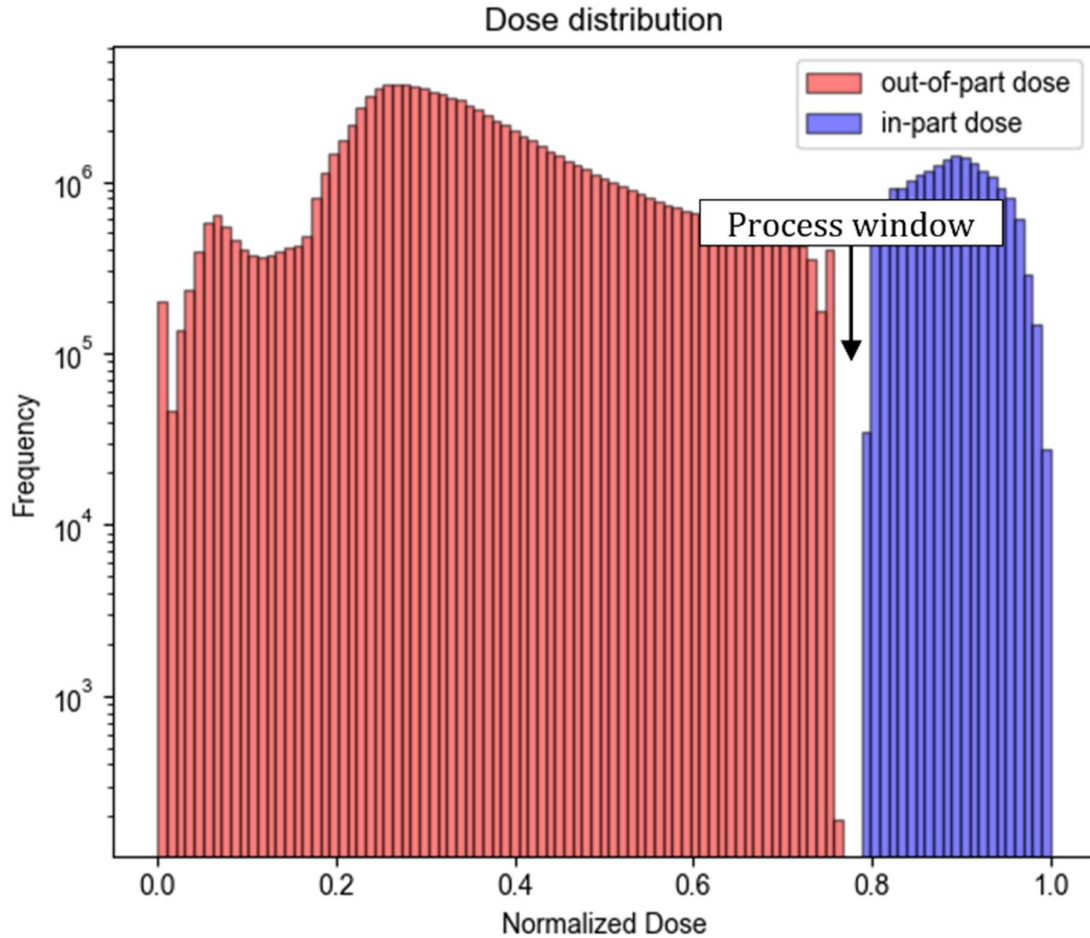


**Figure 4:** Dose distribution histogram of *The Thinker* generated using the OSMO algorithm [19] in VAMToolbox [20]. Optimization parameters:  $D_h=0.8$ ,  $D_l=0.75$ , Iterations=500.

### Results and discussion

For each experiment, twelve print vials were prepared using their respective methods, with the first two being used to determine the time at which to stop the projection by performing test prints which were stopped once the parts appeared to have fully formed. If the printed parts turned out either under- or overcured after post-processing, the print time was then adjusted accordingly in increments of 15 seconds, until a satisfactory print quality was achieved. The increments could potentially have been made smaller to determine the optimal print time more accurately. However, given the limited amount of photopolymer available for the experiments and the large process window provided by the OSMO algorithm, it was decided that increments of 15 seconds were adequate. For the first experiment, the optimal print time was determined to be 2 minutes and 30 seconds and applied to ten consecutive prints, as seen in Fig. 5. In the second experiment, the same initial print time was used as a reference. However, this resulted in a severely undercured print, indicating a higher oxygen concentration in the photopolymer (see Appendix A). Consequently, the print time was increased by 15 seconds to 2 minutes and 45 seconds and used for the subsequent ten prints, as seen in Fig. 6.

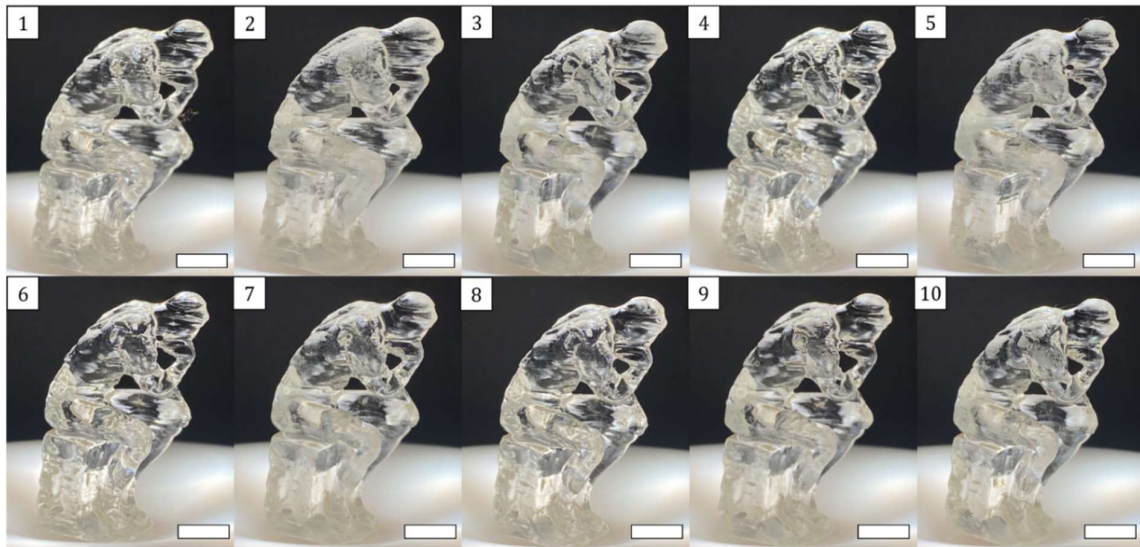


**Figure 5:** Post-processed prints from the first experiment. Scale bars: 5 mm.

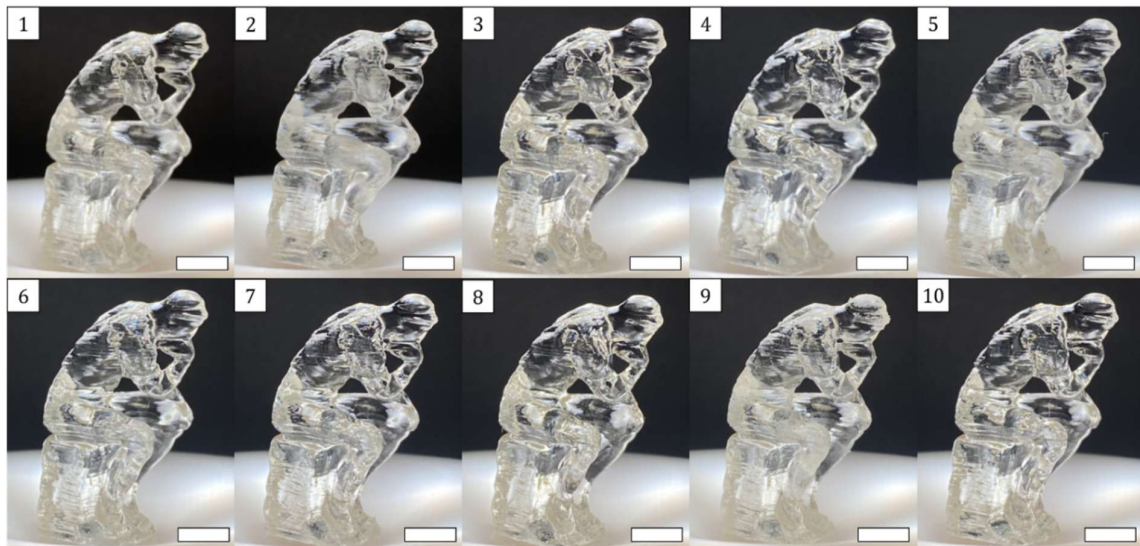


**Figure 6:** Post-processed prints from the second experiment. Scale bars: 5 mm.

Following the two experiments, the inhibition period was determined for each of the prints by carefully analyzing the recordings, as seen in Fig. 7A-C, and noting the curing onset, i.e., the time at which the very first sign of curing was observed. In Table 1, the curing onset for each print can be seen along with a calculation of the associated mean, standard deviation, variance as well as other descriptive metrics.



**Figure 7:** Polymerization progression during printing. (A) Timelapse of print, in increments of approximately 3 seconds from curing onset, (B) first visible sign of curing, (C) finished print suspended within the photopolymer in the print vial. While the polymerization progression of only one print is shown, the head of *The Thinker* was the first region to begin curing in all prints.

**Table 1:** Curing onset time and descriptive metrics from both experiments.

Curing onset [s]			
Print	Experiment #1	Experiment #2	Difference
#1	93	116	23
#2	85	116	31
#3	93	116	23
#4	94	116	22
#5	106	117	11
#6	106	116	10
#7	83	115	32
#8	94	115	21
#9	105	115	10
#10	105	116	11
<b>Mean</b>	96.4	115.8	19.4
<b>Std. Dev</b>	8.67	0.63	8.47
<b>Variance</b>	75.16	0.4	71.82
<b>Minimum</b>	83	115	10
<b>Maximum</b>	106	117	32
<b>Print time</b>	150	165	15

From the results, it is seen that the inhibition period was approximately 20 seconds longer on average and significantly more consistent in the second experiment, where oxygen diffusion

was promoted directly in the print vials to saturate the photopolymer before printing, compared to the first experiment, where the print vials were instead immediately sealed after being filled. In the first experiment, the curing onset varied by a maximum of 23 seconds between the prints, which could indicate an oxygen concentration gradient throughout the container in which the photopolymer is stored. However, since the print vials were used in random order during both experiments, this oxygen concentration gradient cannot be confirmed with certainty, although the observed variation strongly suggests its presence. In hindsight, the print vials could have been numbered and used sequentially given the working principle of the automated filling machine, which most likely would have resulted in the inhibition period increasing gradually during the ten consecutive prints, thereby making it easier to draw conclusions about the presence of any potential oxygen concentration gradient. This could, nonetheless, have also affected the quality of the prints in the first experiment, since the time at which to stop the projection would have been determined using two print vials with a comparatively lower oxygen concentration than the rest, potentially leading to problems with undercuring in the subsequent prints. Regardless, as also evidenced by the high standard deviation, the inconsistent inhibition periods between the print vials in the first experiment still indicate a severely non-uniform oxygen concentration throughout the container in which the photopolymer is stored, which in itself is the primary finding of interest.

In the second experiment, the inhibition period varied by a maximum of only 2 seconds, which, supported by the lower standard deviation, indicates a significantly more uniform oxygen concentration between the print vial, likely caused by the photopolymer becoming fully saturated before printing due to the method of preparation. Arguably, this variation could be within the margin of error. However, it could also result from slight errors in dose delivery due to differences in the borosilicate glass test tubes used as print vials, which could potentially be investigated in future studies.

When examining the surfaces, the quality appears to be similar in both experiments. However, all prints can be seen to be affected by varying degrees of striations due to non-uniform curing and trapped air bubbles in the refractive index matched fluid due to the high viscosity, as also evident in the recordings. While the non-uniform curing is a more complex problem to solve, the trapped air bubbles could be avoided by using a less viscous fluid with a refractive index close to that of the photopolymer, such as mineral oil. However, since the refractive indices are unlikely to match exactly, this would lead to issues with refraction in the plane of curvature of the print vials, which would then need to be managed accordingly.

Upon analyzing the prints by eye, the geometric fidelity of the prints from the second experiment seems to be significantly more uniform and higher than the prints from the first experiment, especially when looking at print #2 in Fig. 5, which appears severely overcured in comparison to print #6 in Fig. 5, despite the projection being stopped at the same time. At first thought, this could simply be explained by the differences in curing onsets between these two prints. However, print #10 in Fig. 5 also appears to be slightly overcured in comparison to print #6 in Fig. 5, despite having the same curing onset and being stopped at the same time, which is seemingly counterintuitive and contradictory. This further emphasizes the challenges associated with inconsistent material properties and the user-induced variation that follows, as it effectively makes the printing process unpredictable and a matter of trial and error. In the second experiment, none of these problems manifest, ultimately cementing saturation of photopolymers with oxygen-mediated inhibition periods before printing as a fundamental prerequisite for ensuring consistency in the printing process, with more uniformity and a higher geometric fidelity of the printed parts to follow.

## **Conclusion**

In this paper, two different methods of preparing the print vials have been employed with the objective of investigating the oxygen concentration within a batch of photopolymer as well as quantifying its effect on the consistency of the printing process. For each method of preparation, two experiments consisting of ten consecutive prints were performed, followed by an analysis of the polymerization progressions captured using in-situ monitoring.

Results show that for photopolymers with oxygen-mediated inhibition periods, a non-uniform oxygen concentration can occur throughout the container in which the photopolymer is stored, leading to inconsistency in the printing process if not addressed. By fully saturating the photopolymer with oxygen directly in the print vials before printing, the inhibition period was increased by approximately 20 seconds on average, while the maximum variation of the curing onset was reduced from 23 seconds without oxygen saturation and 2 seconds with oxygen saturation, indicating a significantly more uniform oxygen concentration between the print vials. This resulted in an improved and significantly more uniform geometric fidelity of the printed parts, while the surface quality remained largely unaffected.

In conclusion, fully saturating the photopolymer before printing ensures consistency in the printing process, helps mitigate user-induced variation, and establishes a foundation for future experimental campaigns where consecutively printed parts can be analyzed qualitatively and compared on a more objective and equal basis.

## **Acknowledgements**

The authors would like to acknowledge the support of the Centre for Acoustic-Mechanical Microsystems (CAMM) at the Technical University of Denmark, sponsored by WSAudiology and Oticon, as well as the Independent Research Fund Denmark (DRF) under Contract No. 0171-00115B.

## **Declarations**

### **Declaration of Competing Interest:**

The authors declare that they have no known competing financial interests or personal relationships that could have appeared to influence the work reported in this paper.

### **Declaration of generative AI and AI-assisted technologies in the writing process:**

During the preparation of this work the authors used Microsoft Copilot in order to improve the readability of the paper. After using this tool/service, the authors reviewed and edited the content as needed and take full responsibility for the contents of the paper

### **Data availability:**

The authors confirm that the data supporting the findings of this study are available within the article. Videos of all recordings made during both experiments are available from the corresponding author, Carl Sander Kruse (cgskr@dtu.dk), upon reasonable request.

## References

- [1] Brett E. Kelly et al. "Computed Axial Lithography (CAL): Toward Single Step 3D Printing of Arbitrary Geometries". (2017).  
<https://doi.org/10.48550/arXiv.1705.05893>
- [2] Brett E. Kelly et al. "Volumetric Additive Manufacturing via Tomographic Reconstruction". In: *Science* 363.6431 (2019), pp. 1075-1079.  
<https://doi.org/10.1126/science.aau7114>
- [3] D. Loterie, P. Delrot, C. Moser. High-resolution tomographic volumetric additive manufacturing, *Nature Communications* 11 (2020) 852. doi:10.1038/s41467-020-14630-4.
- [4] C.M. Rackson, J.T. Toombs, M. P. De Beer, C.C. Cook, M. Shusteff, H.K.Taylor, R.R. McLeod. Latent image volumetric additive manufacturing, *Optics Letters* 47 (5) (2022) 1279—1282. doi:10.1364/OL.449220.
- [5] J.T. Toombs, M. Luitz, C.C. Cook, S. Jenne, C.C. Li, B.E. Rapp, F. Kotz-Helmer, H.K. Taylor. Volumetric additive manufacturing of silica glass with microscale computed axial lithography, *Science* 376 (6590) (2022) 308—312. doi:10.1126/science.abm6459.
- [6] A.F. Wolstrup, J.T. Dagnæs-Hansen, O.V. Brandt, D.H. Meile, C.S. Kruse, J. Spangenberg, T.G. Zsurzsan, Fabrication of conductive structures in volumetric additive manufacturing through embedded 3-d printing for electronic applications, *Additive Manufacturing Letters* 7 (2023) 100178. doi:10.1016/j.addlet.2023.100178.
- [7] M. Kollep, G. Konstantinou, J. Madrid-Wolff, A. Boniface, L. Hagelüken, P. V. W. Sasikumar, G. Blugan, P. Delrot, D. Loterie, J. Brugger, et al., Tomographic volumetric additive manufacturing of silicon oxycarbide ceramics, *Advanced Engineering Materials* 24 (7) (2022) 2101345. doi:10.1002/adem.202101345.
- [8] C. C. Cook, E. J. Fong, J. J. Schwartz, D. H. Porcincula, A. C. Kaczmarek, J. S. Oakdale, B. D. Moran, K. M. Champley, C. M. Rackson, A. Muralidharan, et al., Highly tunable thiol-ene photoresins for volumetric additive manufacturing, *Advanced Materials* 32 (47) (2020) 2003376. doi:10.1002/adma.202003376.
- [9] J. J. Schwartz, D. H. Porcincula, C. C. Cook, E. J. Fong, M. Shusteff, Volumetric additive manufacturing of shape memory polymers, *Polymer Chemistry* 13 (13) (2022) 1813–1817. doi:10.1039/D1PY01723C.
- [10] P. N. Bernal, P. Delrot, D. Loterie, Y. Li, J. Malda, C. Moser, R. Levato, Volumetric bioprinting of complex living-tissue constructs within seconds, *Advanced Materials* 31 (42) (2019) 1904209. doi:10.1002/adma.201904209.
- [11] R. Rizzo, D. Ruetsche, H. Liu, M. Zenobi-Wang, Optimized photoclick (bio)resins for fast volumetric bioprinting, *Advanced Materials* 33 (49) (2021) 2102900. doi:10.1002/adma.202102900.
- [12] D. Webber, A. Orth, V. Vidyapin, Y. Zhang, M. Picard, D. Liu, K. L. Sampson, T. Lacelle, C. Paquet, J. Boisvert. Printing of low-viscosity materials using tomographic additive manufacturing, *Additive Manufacturing* 94 (2024) 104480. doi:10.1016/j.addma.2024.104480.

- [13] T. Waddell, J. Toombs, A. Reilly, T. Schwab, C. Castaneda, I. Shan, T. Lewis, P. Mohnot, D. Potter, H. Taylor. Use of volumetric additive manufacturing as an in-space manufacturing technology, *Acta Astronautica* 211 (2023) 474—482. doi:10.1016/j.actaastro.2023.06.048.
- [14] C. Chung Li, J. Toombs, H. Taylor, Tomographic color Schlieren refractive index mapping for computed axial lithography, In *Proceedings of the 5th Annual ACM Symposium on Computational Fabrication* (12) (2020) 1--7. doi: 10.1145/3424630.3425421
- [15] A. Orth, et al., On-the-fly 3D metrology of volumetric additive manufacturing, *Additive Manufacturing* 56 (2022) 102869. doi:10.1016/j.addma.2022.102869.
- [16] Orth, A., Webber, D., Zhang, Y. et al. Deconvolution volumetric additive manufacturing. *Nat Commun* 14, 4412 (2023). <https://doi.org/10.1038/s41467-023-39886-4>
- [17] T. H. Weisgraber, M. P. de Beer, S. Huang, J. J. Karnes, C. C. Cook, M. Shusteff, Virtual Volumetric Additive Manufacturing (VirtualVAM). *Adv. Mater. Technol.* 2023, 8, 2301054. <https://doi.org/10.1002/admt.202301054>
- [18] Salajeghe, R., Meile, D.H., Kruse, C.S., Marla, D., Spangenberg, J. (2024). Numerical Modeling of Part Formation in Volumetric Additive Manufacturing. In: Klahn, C., Meboldt, M., Ferchow, J. (eds) *Industrializing Additive Manufacturing. AMPA 2023. Springer Tracts in Additive Manufacturing*. Springer, Cham. [https://doi.org/10.1007/978-3-031-42983-5\\_13A](https://doi.org/10.1007/978-3-031-42983-5_13A)
- [19] Charles M. Rackson, Kyle M. Champley, Joseph T. Toombs, Erika J. Fong, Vishal Bansal, Hayden K. Taylor, Maxim Shusteff, and Robert R. McLeod. Object-space optimization of tomographic reconstructions for additive manufacturing. *Additive Manufacturing*, 48:102367, (2021). <https://doi.org/10.1016/j.addma.2021.102367>.
- [20] J. Toombs et al. (2022) "VAMToolbox". <https://vamtoolbox.readthedocs.io>

Appendix

**Appendix A: Undercured initial print in Experiment #2**

